The Encapsidated Genome of *Microplitis demolitor* Bracovirus Integrates into the Host *Pseudoplusia includens*▽‡

Markus H. Beck,† Shu Zhang,† Kavita Bitra,† Gaelen R. Burke, and Michael R. Strand*

Department of Entomology, University of Georgia, Athens, Georgia 30602

Polydnaviruses (PDVs) are symbionts of parasitoid wasps that function as gene delivery vehicles in the insects (hosts) that the wasps parasitize. PDVs persist in wasps as integrated proviruses but are packaged as circularized and segmented double-stranded DNAs into the virions that wasps inject into hosts. In contrast, little is known about how PDV genomic DNAs persist in host cells. *Microplitis demolitor* carries *Microplitis demolitor* bracovirus (MdBV) and parasitizes the host *Pseudoplusia includens*. MdBV infects primarily host hemocytes and also infects a hemocyte-derived cell line from *P. includens* called CiE1 cells. Here we report that all 15 genomic segments of the MdBV encapsidated genome exhibited long-term persistence in CiE1 cells. Most MdBV genes expressed in hemocytes were persistently expressed in CiE1 cells, including members of the *glc* gene family whose products transformed CiE1 cells into a suspension culture. PCR-based integration assays combined with cloning and sequencing of host-virus junctions confirmed that genomic segments J and C persisted in CiE1 cells by integration. These genomic DNAs also rapidly integrated into parasitized *P. includens*. Sequence analysis of wasp-viral junction clones showed that the integration of proviral segments in *M. demolitor* was associated with a wasp excision/integration motif (WIM) known from other bracoviruses. However, integration into host cells occurred in association with a previously unknown domain that we named the host integration motif (HIM). The presence of HIMs in most MdBV genomic DNAs suggests that the integration of each genomic segment into host cells occurs through a shared mechanism.

Viruses in the family *Polydnaviridae* consist of two genera, *Bracovirus* (BV) and *Ichnovirus* (IV), which are symbiotically associated with parasitoid wasps (Hymenoptera) in the families Braconidae and Ichneumonidae (summarized in references 12, 31, 32, and 41). Each polydnavirus (PDV) from a given wasp species is genetically unique and exists in two forms. In the wasp, PDVs persist and are transmitted to offspring as stably integrated proviruses with replication restricted to specialized calyx cells in the ovaries of females. Replication results in the production of the encapsidated form of the virus, which accumulates in the lumen of the calyx. Wasps then inject the encapsidated form of the virus into host insects that they parasitize. For most PDV-carrying wasp species, these hosts are larval-stage Lepidoptera (moths and butterflies). Following parasitism, PDVs do not propagate themselves in the wasp's host because the encapsidated form of the genome lacks most or all of the genes required for replication. However, the encapsidated form of the genome encodes several other genes that alter the development and immune defenses of the host. These alterations in turn enable the wasp's offspring to successfully develop.

The encapsidated genomes of PDVs are segmented and consist of multiple circular double-stranded DNAs that are nonequimolar in abundance (12, 13, 27, 32, 41). In the case of

Microplitis demolitor bracovirus (MdBV), the genome consists of 15 segments (named segments A to O), which are individually packaged into virions and have an aggregate size of 190 kb (5, 42). The encapsidated MdBV genome encodes 51 open reading frames (ORFs) for predicted proteins of ≥100 amino acids (7, 42). More than half of these ORFs form four multimember gene families, designated the *ptp* (13 members), *ank* (12 members), *egf* (3 members), and *glc* (2 members) genes, while the remaining ORFs are predicted single-copy genes (7, 42). Following an infection of the host *Pseudoplusia* (*Chrysodeixis*) *includens*, MdBV virions infect primarily hemocytes as well as other tissues, including the fat body and nervous system (5, 30). Transcripts corresponding to nearly all predicted ORFs are detected in one or more of these tissues within 2 h of infection, with expression thereafter continuing for the 7 days required for *M. demolitor* progeny to complete their development (7, 35, 36). Following wasp emergence, the host larva dies in 2 to 4 days.

While PDV genomes are generally thought to persist in hosts as episomes (28, 38, 41), infection of cell lines with *Glyptapanteles indiensis* bracovirus (GiBV), *Hyposoter fugitivus* ichnovirus (HfIV), and *Hyposoter didymator* ichnovirus (HdIV) suggests that some viral genomic segments persist for long periods by integration (14, 17, 21, 40). The sequencing of host-viral DNA junctions confirmed that one genomic segment from GiBV integrated into two cell lines from the gypsy moth, *Lymantria dispar* (15), while similar data showed that a genomic segment from *Tranosema rostrale* ichnovirus (TrIV) integrated into a cell line from the spruce budworm, *Choristoneura fumiferana* (11). We recently developed a cell line of hemocyte origin from *P. includens*, named CiE1 cells, which is highly permissive to infection by MdBV and exhibits functional

alterations very similar to those of MdBV-infected hemocytes (16). Whether the MdBV genome persists in this cell line, however, is unknown. Here we report that all genomic segments of the MdBV genome persist for long periods in CiE1 cells. Studies focusing on a subset of genomic segments further indicate that persistence is due to integration and that integration also occurs in naturally parasitized *P. includens* larvae.

MATERIALS AND METHODS

Insects and cell lines. *M. demolitor* and *P. includens* were reared at 27°C with a 16-h-light, 8-h-dark photoperiod as previously described (29, 33). Hosts used in the study were parasitized as third-instar larvae. A single wasp offspring emerges from the host's body on day 7 or 8 to pupate within a silken cocoon, followed by emergence into an adult 4 days later (26). CiE1 cells were cultured in Sf-900 medium (Gibco) supplemented with 5% fetal calf serum (HyClone) (16). Non-infected cells were maintained and passaged weekly as strongly adherent cells in Corning 75-cm² tissue culture flasks. MdBV-infected cells became nonadherent but were maintained and passaged identically to noninfected cells.

MdBV collection and nomenclature. MdBV virions were collected from the reproductive tract of adult female wasps in calyx fluid as previously described (2, 35). As is convention in the PDV literature, the amount of MdBV collected from the reproductive tract of a single adult female is defined as one wasp equivalent, which for MdBV contains on average 1×10^{10} virions (5). The encapsidated genome of MdBV was previously deposited in GenBank as individual genomic segments under accession numbers AY887894, AY875680 to AY875690, AY848690, AY842013, and DQ000240 (42). Each genomic segment is named by uppercase letters from smallest (genomic segment A, 3,433 bp) to largest (genomic segment O, 34,355 bp) (42). Nucleotide positions referred to in the study for a given segment correspond to the above-mentioned GenBank submissions, while the abundance of each genomic segment in calyx fluid was previously determined (5). Most predicted genes are named by their location on a given genomic segment (7). Thus, members of the *ptp* gene family consist of one predicted gene located on genomic segment D (*ptp-D1*), five on segment H (*ptp-H1, ptp-H2, ptp-H3, ptp-H4,* and *ptp-H5*), four on segment J (*ptp-J1, ptp-J2, ptp-J3,* and *ptp-J4*), and three on segment N (*ptp-N1, ptp-N2,* and *ptp-N3*) (25, 42). Members of the *ank* gene family are named similarly (*ank-C1, ank-C2, ank-F4, ank-F5, ank-G3, ank-G4, ank-H4, ank-I1, ank-J4, ank-N1, ank-N4,* and *ank-N5*), whereas all *egf* (*egf0.4, egf1.0,* and *egf1.5*) and *glc* (*glc1.8* and *glc3.2*) genes reside on genomic segment O and are named by the size of their corresponding cDNAs (4, 36, 39, 42).

Total RNA isolation and RT-PCR assays. MdBV-infected CiE1 cells were collected by centrifugation at 200 × *g*, followed by the isolation of total RNA using the High Pure RNA isolation kit (Roche) according to the manufacturer's instructions. The quantification of RNA was done by using a Nanodrop spectrometer. For first-strand cDNA synthesis, 100 ng of total RNA was reverse transcribed in 20-μl reaction mixtures using random hexamers and Superscript III (Invitrogen). Reverse transcription (RT)-PCRs were run by using a Bio-Rad thermocycler and 25-μl reaction mixture volumes containing 1 μl of cDNA and 0.2 μM appropriate gene-specific primers. Primers used to amplify selected *ptp* family members were described previously by Pruijssers and Strand (25), primers used to amplify *glc1.8/3.2* and *egf1.0/1.5* were described previously by Beck and Strand (4), and primers used to amplify selected *ank* family members were described previously by Bitra et al. (7). Cycling conditions were as follows: an initial denaturation step at 94°C for 2 min, followed by 35 cycles at 94°C for 20 s, annealing at 50°C (*ptp, glc,* and *egf* genes) or 55°C (all *ank* family members) for 10 s, extension at 65°C for 30 s, and a final extension step at 72°C for 7 min. The resulting products were visualized on 1% agarose gels stained with ethidium bromide (EtBr).

Immunoblotting and immunocytochemistry. MdBV-infected CiE1 cells were placed into lysis buffer and stored at −80°C (20). After protein concentrations were determined by use of the Micro BCA protein assay kit (Pierce), samples were resolved on 4-to-20% gradient SDS-PAGE gels (Lonza), immunoblotted onto a polyvinylidene difluoride (PVDF) membrane (Immobilon-P; Millipore), and blocked (20). The membrane was probed with a murine monoclonal antibody (55F2E7) specific for Glc1.8 and Glc3.2 (1:10,000 dilution) (2, 39). The primary antibody was detected by using a goat anti-mouse horseradish peroxidase-conjugated secondary antibody (1:20,000 dilution) (Jackson Laboratory), followed by visualization using a chemiluminescent substrate (ECL Advance kit; GE Healthcare) (20). MdBV-infected CiE1 cells were processed for immunofluorescence microscopy as previously outlined (3), by labeling with an anti-

Glc1.8/3.2 antibody and an anti-mouse Alexafluor 564-conjugated secondary antibody. Samples were examined by using a Leica IRE2 inverted epifluorescence microscope interfaced (Compix, Cranberry, PA) with SimplePCI software and a Hamamatsu digital camera for image acquisition. Final images were assembled by using Adobe Photoshop.

DNA isolation and PCR-based detection of MdBV genomic segments. Genomic DNA from adult male *M. demolitor*, MdBV-infected CiE1 cells, whole parasitized *P. includens* larvae (7 days postoviposition), or hemocytes from parasitized *P. includens* larvae (2 h to 8 days postparasitism) was isolated by using the QIAamp DNA minikit (Qiagen). For whole parasitized larvae, no *M. demolitor* offspring were present in the sample. MdBV genomic DNA was isolated from virions as previously described (35). Genomic DNA isolated from noninfected CiE1 cells or nonparasitized *P. includens* also served as controls for some experiments. The detection of each MdBV segment in infected CiE1 cells by PCR was conducted by using segment-specific primers as previously described (5). A PCR-based integration assay (1) was used to locate domains of MdBV genomic segments B, C, and J that contained the proviral excision/integration site in *M. demolitor* and the site of integration into CiE1 cells and *P. includens* larvae. Briefly, segments B and C were divided into 4 domains and segment J was divided into 5 domains by designing overlapping primer pairs that specifically amplified each region (see Table S1 in the supplemental material). PCRs were then run in 25-μl reaction mixtures containing 0.2 μM each domain-specific primer; 10 ng of MdBV, *M. demolitor,* CiE1, or *P. includens* DNA; and 1.25 units of Hotmaster *Taq* polymerase (5 Prime). Cycling conditions were as follows: an initial denaturation step at 94°C for 2 min, followed by 35 cycles of denaturation at 94°C for 20 s, annealing at 50°C for 20 s, and extension at 65°C for 4 min, with a final extension step at 72°C for 7 min.

Inverse PCR. We used inverse PCR (22) to amplify, clone, and sequence DNA junctions where a given MdBV segment had integrated and joined with flanking *M. demolitor,* CiE1, or *P. includens* chromosomal DNA. On the basis of our integration assay data (see Results), nested inverse PCR primer sets for MdBV segments C and J (see Table S2 in the supplemental material) were designed based on the domains identified as the site of integration into *M. demolitor,* CiE1 cells, or parasitized *P. includens.* We then digested 5 μg of *M. demolitor,* CiE1, or *P. includens* genomic DNA with MfeI and XbaI for the cloning of right and left virus junctions of segment B from *M. demolitor,* CiE1 cells and *P. includens* for segment C, and PciI for the left junctions for segment J. Following phenol extraction and ethanol precipitation, precipitated DNAs were resuspended in 10 mM Tris-HCl (pH 8.5), diluted to 2 ng/μl, and used for ligation reactions with T4 DNA ligase (Roche) at 10°C overnight. After ligation, the T4 DNA ligase was heat inactivated at 65°C for 10 min, and 1 μl of the reaction mixture was used as template DNA for the first of three consecutive rounds of 50-μl standard PCR amplifications employing Hotmaster *Taq* DNA polymerase (5 Prime) and 0.4 μM segment-specific primers (see Table S2 in the supplemental material). Cycling conditions were as follows: an initial denaturation step at 94°C for 2 min, followed by 35 cycles of denaturation at 94°C for 20 s, annealing at 50°C for 20 s, and extension at 65°C for 3 min. After the first round of amplification employing the outer primer set, 1 μl of the PCR mixture was used to set up a second round of amplification with the same primers. One microliter from this reaction mixture was then used for a third round of amplification with the nested primer pair. The resulting PCR products from the final amplification were cloned with the StrataClone PCR cloning kit (Stratagene) and sequenced using M13 forward and reverse primers (Macrogen). Sequences were analyzed by using DNAStar (Madison, WI) and BLAST (NCBI).

qPCR and Southern blotting. To measure the copy numbers of MdBV segments C and J per infected CiE1 cell, total genomic DNA was isolated from 1×10^6 cells as described above, followed by quantitative PCR (qPCR) analysis using segment C-specific (5′-TATGATGATTTGCCGTAAGGGTAA-3′ [forward] and 5′-AGTAGGCCATGTGGTAAGCAGTAT-3′ [reverse]) and segment J-specific (5′-CCAATTCGGAAGGGTCTCG-3′ [forward] and 5′-GGGGTAGCACTTTTGTTTGTTATCT-3′ [reverse]) primers as previously described (5). For Southern blotting, digoxigenin-labeled probes corresponding to nucleotides (nt) 4077 to 5866 on segment C and nt 5409 to 8215 on segment J were synthesized by using digoxigenin-dUTP and DIG High Prime DNA Labeling and Detection Start kit II (Roche). MdBV genomic DNA isolated from virions and CiE1 genomic DNA were digested with XbaI (segment C) or BspHI (segment J), followed by size fractionation on 0.8% agarose gels and transfer onto nylon in 20× SSC (1× SSC is 0.15 M NaCl plus 0.015 M sodium citrate). Blots were then prehybridized for 30 min at 40°C in DIG Easy Hyb buffer (Roche), followed by overnight hybridization at 40°C with each probe (30 ng/ml). Blots were washed under conditions of high stringency (0.5× SSC, 0.1% SDS) at 65°C, followed by incubation with antidigoxigenin antibody (Roche) (1:10,000) and visualization using the CSP-Star ready-to-use chemiluminescent substrate (Roche).
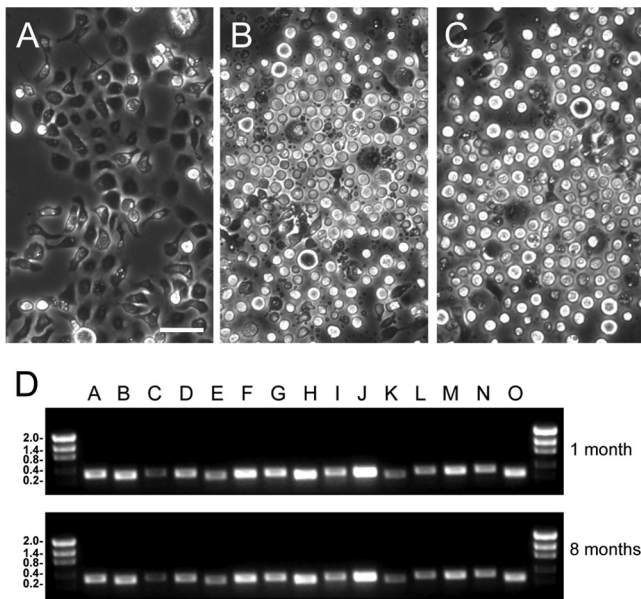
FIG. 1. MdBV persists in and transforms CiE1 cells. (A) Phase-contrast micrograph of uninfected CiE1 cells. Note that cells are strongly adhered to and spread on the surface of culture plates. The scale bar equals 100 μm. (B) Phase-contrast micrograph of CiE1 cells 72 h after infection by MdBV. (C) Phase-contrast micrograph of CiE1 cells 8 months after infection by MdBV. Inspection of panel B shows that most cells are rounded and that numerous small blebs are present due to apoptosis, while panel C shows that most cells remain rounded but that few blebs are present. (D) PCR products generated using DNA from infected CiE1 cells as a template and primers specific for each MdBV genomic segment (segments A to O). The top gel shows products produced from CiE1 cells 1 month postinfection, while the bottom gel shows products generated from CiE1 cells 8 months postinfection. Size markers (kb) are shown at the left.

RESULTS

MdBV persists in and functionally transforms CiE1 cells. A key function of PDVs in parasitism is to prevent the host's immune system from killing the progeny (eggs and/or larvae) of parasitoids by a cellular defense response called encapsulation (summarized in references 31 and 32). MdBV disables encapsulation by preventing hemocytes called granulocytes and plasmatocytes from adhering to wasp eggs and causing some granulocytes to apoptose (33, 34, 39). The loss of adhesion is due primarily to the expression of the *glc* genes in infected hemocytes, which encode very similar cell surface glycoproteins (3, 4, 25), while apoptosis is associated with the expression of *ptp-H2* (37). We also previously showed that MdBV infection blocks adhesion and causes some CiE1 cells to apoptose, while the RNA interference (RNAi) knockdown of *glc* gene expression rescues adhesion (16). At the beginning of this study, we infected CiE1 cells with MdBV at an average multiplicity of infection (MOI) of 10, which resulted in most cells becoming nonadhesive and some cells apoptosing at between 24 and 72 h, as previously reported (Fig. 1A and B). However, apoptosis thereafter declined, with surviving cells remaining nonadhesive but also proliferating at rates comparable to those of uninfected cells. We therefore maintained these cells by passaging them weekly. Strikingly, cells remained nonadhesive after 1 month and 4 passages as well as after 8

months and 39 passages (Fig. 1C). PCR assays using DNA isolated from CiE1 cells as a template and primers specific for each MdBV genomic segment further indicated that each segment persisted over the same period (Fig. 1D).

Multiple MdBV genes are persistently expressed in CiE1 cells. Transcriptome analysis previously showed that a majority of the MdBV *ptp*, *ank*, *glc*, and *egf* gene family members are expressed in *P. includens* hemocytes (7). Given that CiE1 cells were transformed from an adhesive to a nonadhesive state after infection and all MdBV genomic segments persisted, we qualitatively assessed by RT-PCR whether the persistent expression of MdBV genes also occurred. Our results showed that most viral gene family members expressed in *P. includens* hemocytes, including the *glc* genes responsible for adhesion loss, continued to be expressed in CiE1 cells after 1 and 8 months (Fig. 2A). In contrast, no amplicons for these gene products were detected in noninfected CiE1 cells (not shown). Immunoblot analysis using an anti-Glc1.8/3.2 antibody detected the presence of both Glc1.8 and Glc3.2 in cell extracts prepared at 1 month postinfection but detected only Glc3.2 at 8 months postinfection (Fig. 2B). Immunocytochemical analysis also showed that virtually all CiE1 cells at 8 months postinfection expressed Glc3.2 on their surface (Fig. 2C).

MdBV genomic segments B, C, and J persist in CiE1 cells by integration. Since the encapsidated form of the MdBV genome cannot replicate, we asked whether MdBV genomic segments persisted in CiE1 cells as episomes or by integration. We selected the most (segment J) and least (segment C) abundant segments of the genome (5) plus a segment of intermediate abundance (segment B) for further study by designing overlapping primer pairs to amplify specific domains of each segment unless linearized and integrated (Fig. 3). We then compared amplification products using these primers and the following templates: (i) episomal viral DNA isolated from virions; (ii) genomic DNA from male *M. demolitor* wasps, which contain primarily the proviral (integrated) form of MdBV; and (iii) genomic DNA from CiE1 cells infected 21 days earlier by MdBV. As expected, we amplified each domain of segments B, C, and J using episomal viral DNA as a template (Fig. 3). In contrast, we generated no amplicons for domains 2 and 3 of segment B from male wasp DNA and MdBV-infected CiE1 DNA (Fig. 3A). For segment C, we generated no amplicon for domain 1 from male wasp and CiE1 DNAs (Fig. 3B), while for segment J, we generated no amplicon for domain 1 from male wasp DNA and no amplicons for domain 1 or 2 from CiE1 DNA (Fig. 3C). Identical results were generated by using DNA isolated from CiE1 cells at 8 months and 12 months postinfection (not shown). Taken together, these data strongly suggested that segments B, C, and J persisted in CiE1 cells by integrating within 21 days of infection and that no segments persisted as episomes. These data also suggested that integration occurred in domains on each segment that also contained the site of integration of proviral segments B, C, and J in *M. demolitor*.

A proviral excision/integration motif identifies the site of integration of MdBV genomic DNAs into *M. demolitor* but not CiE1 cells. The tetramer AGCT embedded within a larger motif was previously identified as the site of excision for proviral genomic segments of GiBV and *Glyptapanteles flavicoxis* bracovirus (GfBV) from their associated wasps (10). Similar
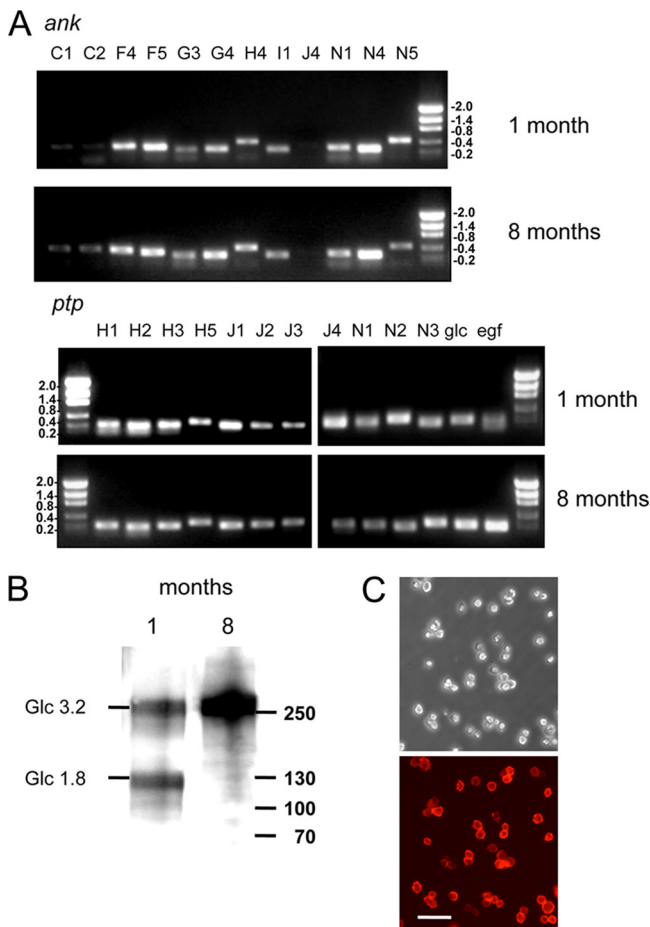
FIG. 2. MdBV transcripts are persistently detected in infected CiE1 cells. (A) Total RNA was isolated from CiE1 cells at 1 and 8 months postinfection, followed by RT-PCR analysis using primers specific for selected *ank* and *ptp* gene family members. Primers that amplify both *glc1.8/3.2* and *egf1.0/1.5* were also used. Amplicons for most genes were detected at both 1 and 8 months postinfection. Size markers (kb) are indicated to the right or left of the gels. (B) Immunoblot showing the presence of Glc1.8 and Glc3.2 in CiE1 cell extracts 1 month postinfection and the presence of only Glc3.2 in cells at 8 months postinfection. Molecular mass markers (in kDa) are indicated at the right. (C) Phase-contrast (top) and epifluorescence (bottom) micrographs of CiE1 cells at 8 months postinfection labeled with anti-Glc1.8/3.2 and visualized by using an Alexa 564 secondary antibody. The scale bar in the bottom image equals 180 μm.

sequences have also been identified in some proviral genomic segments from *Chelonus inanitus* bracovirus (CiBV) (1). Here we refer to these domains as the predicted wasp excision/integration motif (WIM). Since all BVs evolved from a common ancestor (6, 43), we assessed whether such motifs existed within the larger domains on MdBV segments B, C, and J where integration into the genome of *M. demolitor* and CiE1 cells occurred. Our analysis confirmed the presence of a predicted WIM in each of these genomic segments as well as in several others (Fig. 4A). Sequences to 36 nt upstream of the AGCT tetramer were AT rich and highly conserved among segments, whereas sequence conservation was weaker downstream of the AGCT tetramer (Fig. 4A).

To assess whether these motifs identified the site of integra-

tion into *M. demolitor* and CiE1 cells, we conducted PCR-based integration assays using primers that flanked the WIMs on segments B, C, and J (Fig. 4B). In control assays, PCR products of the expected size were amplified by using episomal MdBV DNA as a template (Fig. 4B). In our treatment assays, no products were generated from male wasp DNA, whereas products were generated for each segment using CiE1 cell DNA as a template (Fig. 4B). Together, these data indicated that the predicted WIM on these MdBV segments identified the site of integration into *M. demolitor* but did not identify the site of integration into CiE1 cells. To confirm that integration into *M. demolitor* corresponded precisely with the WIM, we used nested primers; MfeI-, XbaI-, or PciI-digested *M. demolitor* DNA; and inverse PCR to amplify, clone, and sequence wasp-proviral junction sequences for segments B and J. Sequencing of the clone MdB1R identified the right junction for proviral segment B (Fig. 4C). The AGCT tetramer identified the boundary for proviral segment B, which was then followed by 132 bp of *M. demolitor* genomic sequence (Fig. 4C). Reciprocally, sequencing of the clone MdJ1L identified the left junction for proviral segment J where the tetramer AATT formed the boundary followed by 426 bp of *M. demolitor* genomic sequence (Fig. 4C).

Sequencing of host-viral DNA junctions confirms that segments J and C integrate into CiE1 cells and parasitized *P. includens*. To narrow the location on segments B, C, and J where integration into CiE1 cells occurred, we used other primer pairs within the domains identified in Fig. 3 and conducted additional PCR-based integration assays. Our results indicated that segment B integrated into CiE1 cells at a region between nucleotides (nt) 4440 and 4660, segment C integrated between nt 1931 and 3161, and segment J integrated between nt 3050 and 3558 (data not shown). We then used these results to design nested primer sets for use in inverse PCRs to clone and sequence CiE1-viral DNA junction sequences. We identified two left junction clones (CiJ1L and CiJ2L) and one right junction clone (CiJ1R) that corresponded to CiE1-segment J integration sequences (Fig. 5A). The boundaries of both left junction clones corresponded to nt 3262 on segment J and the tetramer ACCA, while the right boundary of the right junction clone corresponded to nt 3211 and the tetramer TAGT. These data also indicated that integration was associated with a ca. 50-bp deletion of segment J. BLAST analysis of the CiE1 flanking sequences for both the left and right junction clones revealed no significant homology with other sequences in current databases. We also identified one right junction clone (CiC1R) for a CiE1-segment C integration event (Fig. 5B). The boundary of this junction corresponded to nt 2673 on segment C and the tetramer TAGT, which was identical to the boundary identified for the right junction of segment J. CiE1 flanking sequences associated with segment C shared no homology with known sequences in current databases and also differed from the flanking sequences associated with the integration of segment J.

We assessed whether MdBV genomic segments integrated into naturally parasitized *P. includens* by first isolating genomic DNA from host hemocytes at day 7 postparasitism and conducting PCR-based integration assays with segments B, C, and J as described above for CiE1 cells. Our results suggested that segments B and C had integrated due to the absence of am-
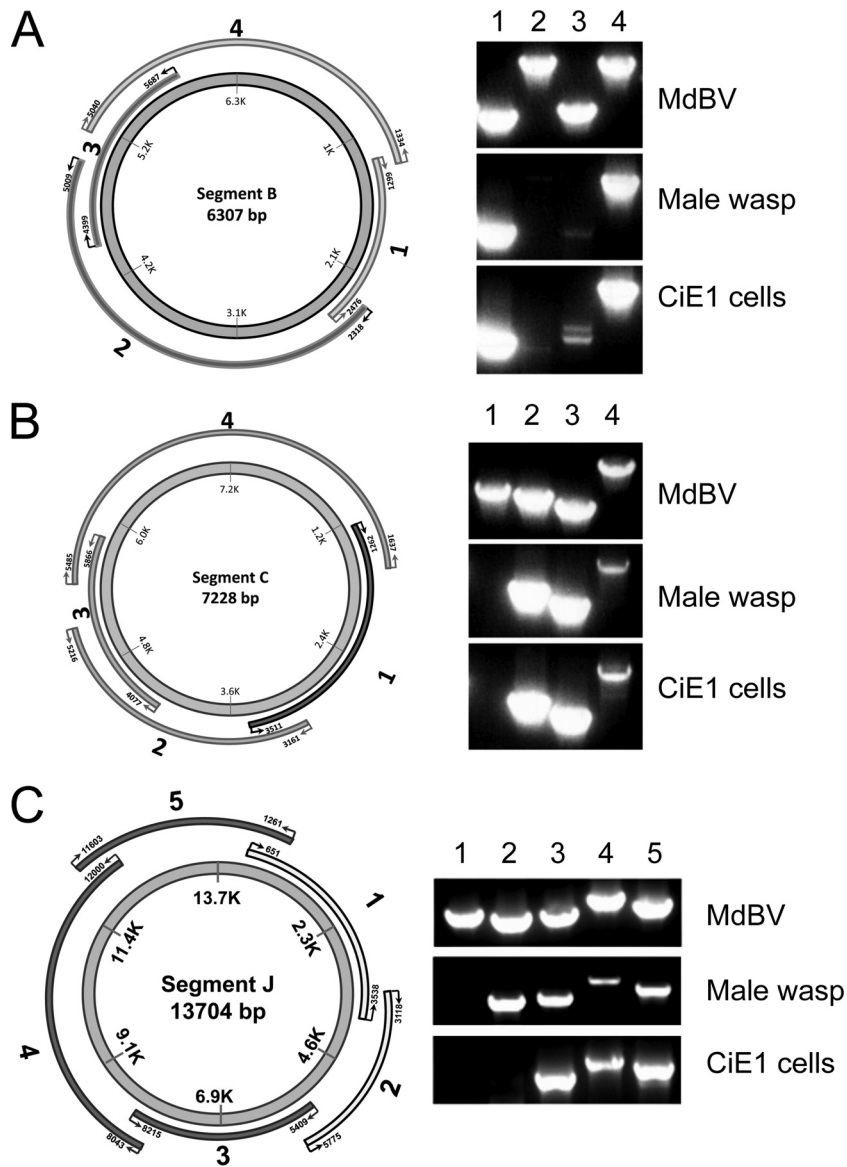
FIG. 3. MdBV genomic segments B, C, and J are integrated into adult male *M. demolitor* and CiE1 cells 21 days after infection with MdBV. Panels A to C show the designs and outcomes of PCR-based integration assays for segments B, C, and J, respectively. The schematics to the left show each genomic segment, with the inner circles indicating segment sizes (bp) and the outer bands indicating the locations of primers used to amplify different domains of each segment. To the right of each schematic are the PCR products generated using the domain-specific primers and DNA from MdBV, adult male *M. demolitor*, or 21-day-postinfection CiE1 cells. Numbers above each lane correspond to the domains shown in each schematic.

plicons for domains 2 and 3 with segment B and an absence of domain 1 for segment C (Fig. 6A). In contrast, the detection of amplicons for each domain of segment J suggested that episomal DNA remained present (Fig. 6A). However, the reduced band intensity for domains 1 and 2 also suggested that some copies of segment J had potentially integrated (Fig. 6A). Additional assays conducted with segment B and DNA isolated from host hemocytes at earlier time points postparasitism suggested that integration had begun by 36 h, as evidenced by the reduced band intensities for domains 2 and 3 (not shown). By 120 h (5 days) postinfection, however, all copies of segment B appeared to be integrated, as evidenced by a failure to amplify domains 2 and 3, as shown in Fig. 6A. We then isolated

genomic DNA from whole host larvae at day 7 postparasitism, followed by the cloning and sequencing of inverse PCR products under reaction conditions that were identical to those used for CiE1 cells. Note that no wasp offspring were present in these samples. One left junction sequence (clones PiJ1L and PiC1L) and one right junction sequence (clones PiJ1R and PiC1R) were identified for both segments J and C (Fig. 6B and C). As with CiE1 cells, the left and right boundaries for segment J corresponded to nt 3262 and 3211, while the left and right boundaries for segment C corresponded to nt 2725 and 2673. Host flanking sequence data also shared no homology with known sequences in databases.

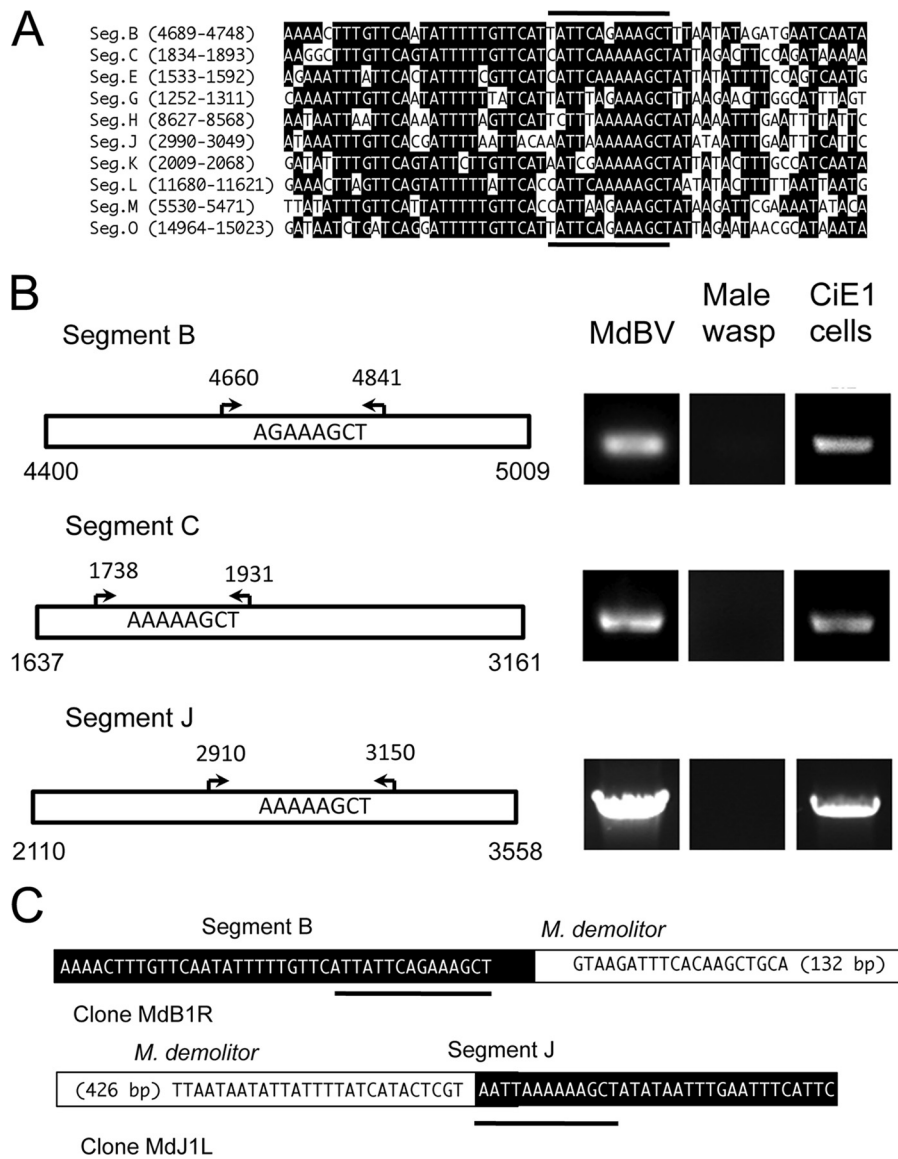However, by comparing the cloned junctions for segment J

FIG. 4. A wasp excision/integration motif (WIM) identifies the site of integration of MdBV genomic segments B, C, and J in *M. demolitor* but not CiE1 cells. (A) Alignment of the predicted WIM on selected MdBV genomic segments. The location of the motif on each segment is indicated at the left. Identical nucleotides are indicated in black. The dark lines above and below the alignment indicate the predicted sites of integration of the corresponding proviral DNA in *M. demolitor*. (B) Outcome of PCR-based integration assays. Schematics to the left show larger domains on segments B, C, and J where the predicted WIM is located. Arrows and corresponding nucleotides identify the locations of flanking primers used in PCR-based integration assays. To the right of each schematic are the PCR products generated using these primers and DNA from MdBV, adult male *M. demolitor*, or CiE1 cells infected 21 days earlier with MdBV as a template. (C) Schematics illustrating the right segment B-*M. demolitor* junction sequence and left segment J-*M. demolitor* junction sequence cloned by inverse PCR. The MdBV sequence is highlighted in black, and the *M. demolitor* genomic sequence is highlighted in white. Note that the right boundary border for segment B is identified by the tetramer AGCT, while the right boundary for segment J is identified by the tetramer AATT, as shown by the black underlining in panel A. The cloned and analyzed *M. demolitor* sequence flanking segment B is 132 bp, while the sequence for segment J is 426 bp.

to one another, we determined that a portion of clone CiJ1R from CiE1 cells was identical to clones PiJ1R and PiJ1L from parasitized *P. includens*. We aligned these clones with one another in Fig. 7A, which shows that three copies of segment J integrated within a 1,285-bp domain in the genome of CiE1 cells and parasitized *P. includens* that we call a putative host target site. By arbitrarily designating position 0 the site of insertion for segment J in the right junction clone from CiE1 cells (CiJ1R), Fig. 7A shows that segment J for the right junc-

tion clone (PiJ1R) from *P. includens* was integrated 354 bp upstream, while segment J for the left junction clone (PiJ1L) from *P. includens* was integrated 43 bp downstream. Figure 7A also shows that segment J was integrated in one orientation (flip) for the right junction clones from CiE1 cells and *P. includens* but was integrated in the opposite orientation (flop) for the left junction clone from *P. includens*. We assembled the sequence of the presumptive host target site from the flanking sequence data of the three clones. The region overall exhibited
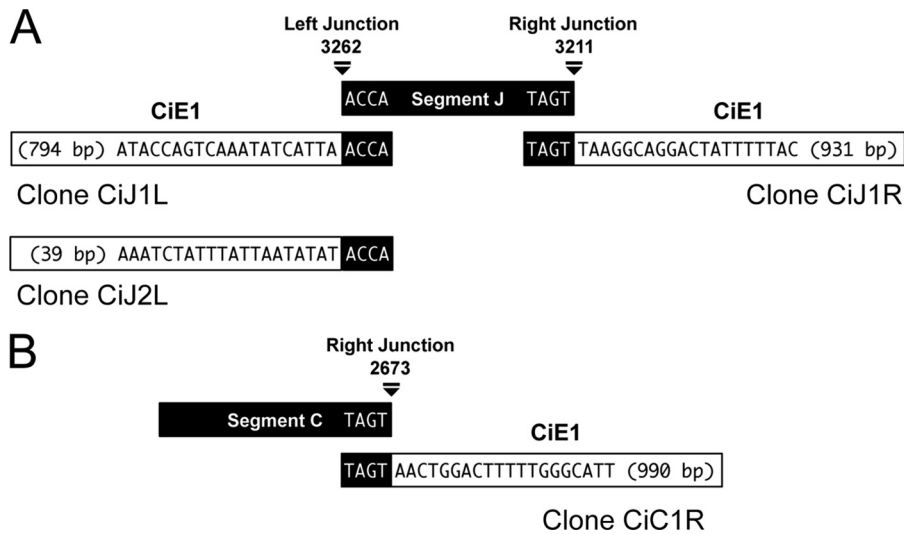
FIG. 5. Inverse PCR clones confirm that MdBV segments J and C integrate into the genome of CiE1 cells. (A) Schematic illustrating the two left (CiJ1L and CiJ2L) and one right (CiJ1R) segment J-CiE1 junction sequences cloned by inverse PCR. Each junction clone is aligned with segment J linearized at nt 3262 (left) and nt 3211 (right). The MdBV sequence in each junction clone is highlighted in black, and the CiE1 genomic sequence is highlighted in white. Note that the segment J boundary for both left clones corresponds to nt 3262 and the tetramer ACCA, while the boundary for the right junction clone corresponds to nt 3211 and the tetramer TAGT. The analyzed CiE1 sequences for the two left junction clones are 794 and 39 bp long, respectively, while the CiE1 sequence for the right junction clone is 931 bp. (B) Schematic illustrating the one right (CiC1R) segment C-CiE1 junction sequence cloned by inverse PCR. The schematic is organized as described above (A). The CiE1 sequence for the clone is 990 bp.

a high A+T content (64%) and showed that each copy of segment J was inserted at sites identified by the sequence TA or TTA but shared no obvious homology with the boundary sequences for segment J (Fig. 7A). Examination of the host

sequences for the two left junction clones (CiJ1L and CiJ2L) (Fig. 5) for segment J from CiE1 cells indicated that they shared no sequence homology with one another or the host target site shown in Fig. 7A. The host sequences from the two
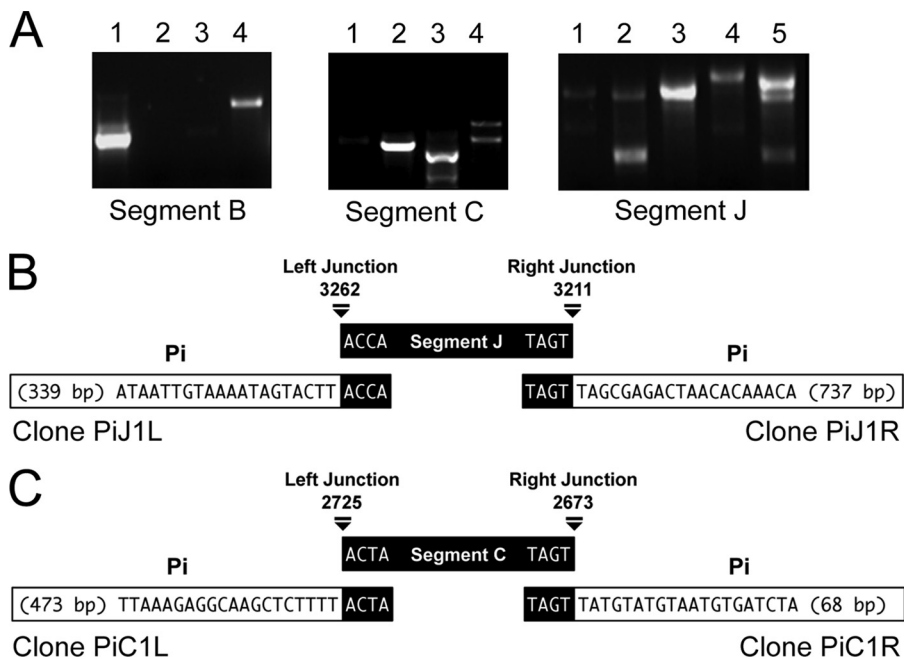

FIG. 6. PCR-based integration assays and inverse PCR clones confirm that MdBV segments integrate into the genome of parasitized *P. includens*. (A) PCR products amplified using domain-specific primers for segments B, C, and J and hemocyte genomic DNA collected from parasitized *P. includens* larvae (day 7 postparasitism). Domains correspond to the domains shown in Fig. 3. (B) Schematic illustrating the one left (PiJ1L) and one right (PiJ1R) segment J-*P. includens* junction sequences cloned by inverse PCR. The schematic is organized as described in the legend of Fig. 5. The *P. includens* (Pi) sequence for the left junction clone is 339 bp long, while the *P. includens* sequence for the right junction clone is 737 bp. (C) Schematic illustrating the one left (PiC1L) and one right (PiC1R) segment C-*P. includens* junction sequences cloned by inverse PCR. The *P. includens* sequence for the left junction clone is 473 bp long, while the *P. includens* sequence for the right junction clone is 68 bp.
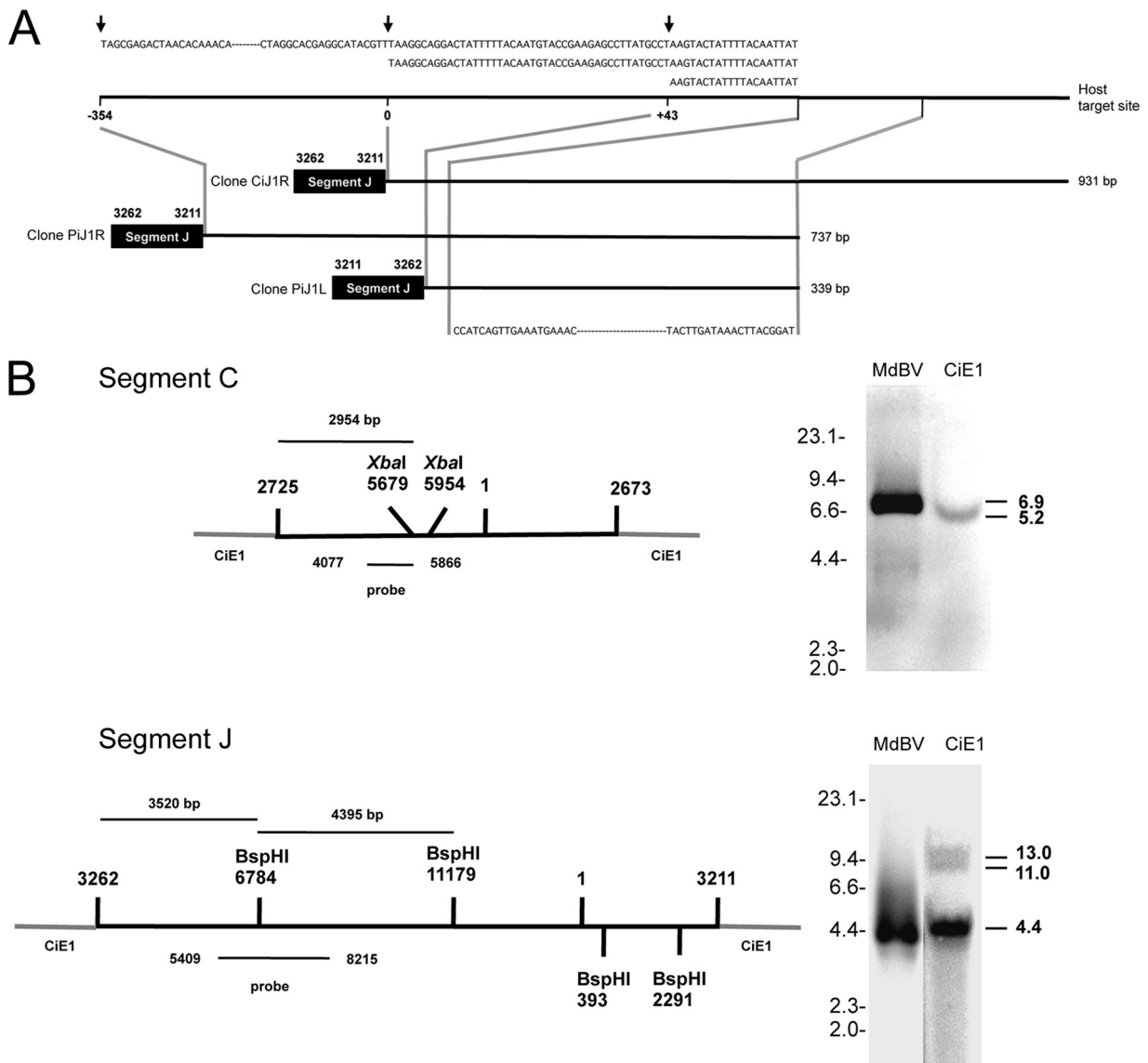
FIG. 7. Integration of MdBV genomic DNAs is nonrandom. (A) Schematic showing that segment J-host junction clones CiJ1R (931 bp), PiJ1R (737 bp), and PiJ1L (339 bp) integrate into the same target site in CiE1 cells and *P. includens*. The integration of segment J from clone CiJ1R is shown at position 0 in the host target site. Segment J from clone PiJ1R is inserted at position −354, while segment J from clone PiJ1L is inserted at position +43. Above each clone is the sequence of the deduced host target site, with arrows indicating where each copy of segment J integrated. Below each clone is the region in each clone that was fully identical. (B) Southern blot analysis of MdBV and CiE1 genomic DNAs probed with a segment C-specific (above) or segment J-specific (below) probe. The schematics at the left show segments C and J integrated into CiE1 genomic DNA, as determined by the sequencing of junction clones (Fig. 5 and 6). XbaI (segment C) and BspHI (segment J) sites are indicated, as is the site within each segment that corresponds to the probes that we synthesized. At the right are Southern blots of XbaI-digested MdBV and CiE1 genomic DNAs hybridized with the segment C probe (above) or BspHI-digested MdBV and CiE1 genomic DNAs hybridized with the segment J probe (below). Size markers (kb) are indicated to the left of each blot, while the estimated sizes (kb) of the fragments recognized by each probe are indicated at the right.

junction clones for segment C (PiC1L and PiC1R) (Fig. 5) from *P. includens* also shared no homology with one another or the putative host target site for segment J.

To further characterize integration into CiE1 cells, we conducted qPCR assays to estimate the average copy numbers per cell for segments C and J and Southern blotting experiments to determine whether integration occurred in one or more locations in the genome. Our qPCR results indicated that 1.03 ± 0.13 copies of segment C were present on average per CiE1 cell

at 8 months postinfection, while 21.03 ± 0.1 copies of segment J were present. If these segments randomly integrated into the genome of CiE1 cells, we would expect to observe a large number of bands or a smear on Southern blots. We digested MdBV and CiE1 genomic DNAs with XbaI, for which there are two predicted cut sites in segment C (Fig. 7B). In turn, the segment C probe that we generated should hybridize to a 6.9-kb fragment of segment C if not integrated but should recognize a 2.95-kb region of segment C plus an unknown
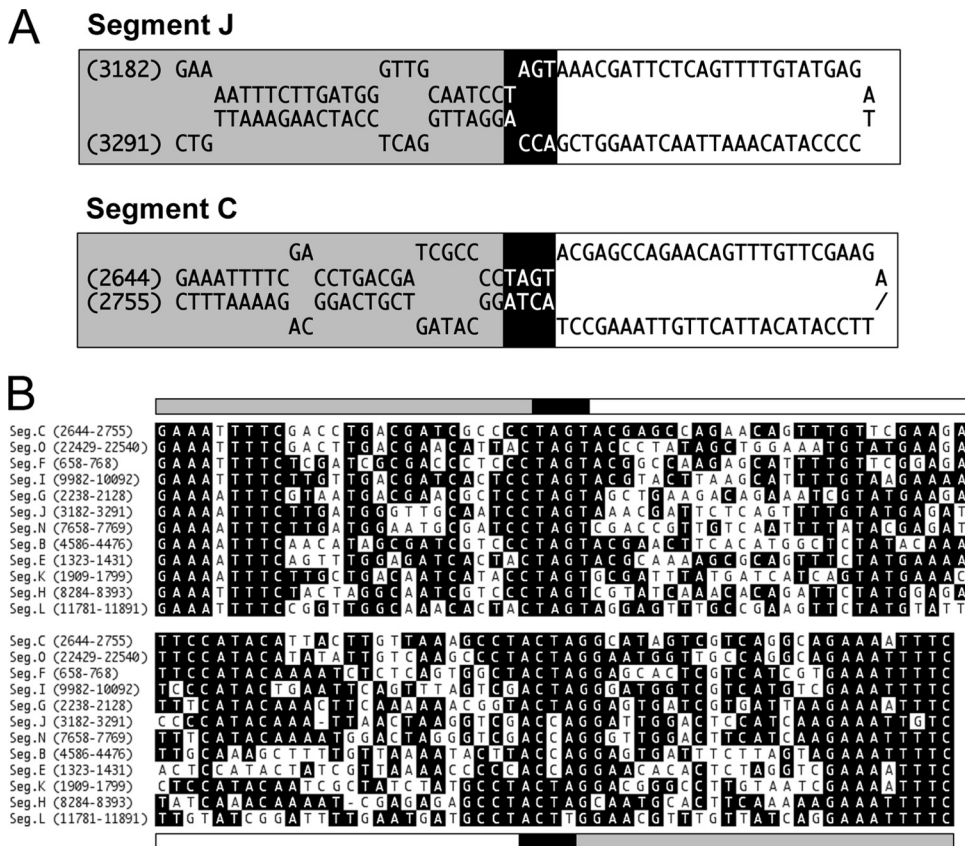
FIG. 8. MdBV genomic DNAs contain similar host integration motifs (HIMs). (A) Predicted stem-loop structures for the segment J and C HIMs generated by Mfold. Gray highlights nucleotides that form the base of the stem, black highlights the tetramers that identify the boundary site of integration of each segment into host cells, and white highlights the predicted loop domain that is deleted with integration into the host genome. (B) Sequence alignment of the HIMs from selected MdBV genomic segments. The position of the motif on each segment is indicated at the left. Identical nucleotides are indicated in black. The gray, black, and white lines above and below the alignment correspond to the stem and loop regions shown in panel A.

length of flanking CiE1 genomic DNA if integrated as shown in Fig. 5 and 6. Our results indicated that this probe recognized the predicted 6.9-kb fragment of nonintegrated segment C when hybridized to MdBV genomic DNA and a single 5.2-kb fragment when hybridized to CiE1 genomic DNA (Fig. 7B). We then digested CiE1 and MdBV genomic DNAs with BspHI, for which there are four predicted cut sites in segment J (Fig. 7B). The segment J probe that we generated should hybridize to two 4.4-kb fragments of MdBV segment J if not integrated but should recognize a 4.4-kb fragment and a 3.5-kb region of segment J plus an unknown length of flanking CiE1 genomic DNA. Our results showed that this probe recognized the predicted 4.4 kb-fragments of nonintegrated segment J when hybridized to MdBV genomic DNA (Fig. 7B). When hybridized to CiE1 genomic DNA, the probe also recognized the predicted 4.4-kb fragment plus two other bands of approximately 13.0 and 11.0 kb (Fig. 7B). Overall, these results clearly indicated that segments J and C integrate into both CiE1 cells and parasitized *P. includens* larvae and that integration is associated with near-identical boundary sequences on each of these viral segments. In addition, these results also suggested that segments C and J do not integrate randomly into the *P. includens* genome.

MdBV segments share a host integration motif. Given the near-identical boundary sequences associated with the integration of segments J and C into host cells, we asked whether similarities also existed in terms of where on each segment integration occurred. Indeed, the site of integration on each segment corresponded to a 110- or 111-nt domain consisting of two imperfect inverted repeats, which formed predicted stem-loop structures using Mfold 3.2 (45), to optimize base pairing (Fig. 8A). A comparison of these stem-loop structures to our junction sequence data further showed that the integration boundary for each segment and every clone that we sequenced corresponded with the deletion of the 50-nt (segment J) or 51-nt (segment C) loop. This deletion in turn resulted in the tetramer ACCA or ACTA forming the left border with the host genome and TAGT forming the right border. An examination of other MdBV genomic segments revealed the presence of similar domains comprised of conserved inverted repeats and a more variable loop region (Fig. 8B). We therefore named this domain the MdBV host integration motif (HIM). Consistent with our PCR-based integration assay data (Fig. 3), the HIM and WIM were located in close proximity (109 to 168 nt) to one another on segments B and J as well as most other MdBV genomic DNAs (Table 1). However, these motifs were

TABLE 1. Location of the predicted host integration motif
compared to the predicted wasp excision/integration
motif on selected MdBV genomic segments[a]

Segment (size [nt])	Positions of host integration motif	Positions of wasp excision/integration motif	Proximity (nt)
B (6307)	4586–4476	4699–4728	112
C (7228)	2644–2755	1844–1873	770
E (8443)	1323–1431	1543–157	111
G (10,790)	2238–2128	1262–1291	836
H (11,238)	8284–8393	8562–8591	168
J (13,704)	3182–3291	3055–3026	126
K (15,058)	1909–1799	2019–2048	109
L (15,096)	11781–11891	11670–11641	110
M (15,218)	5697–5798	5520–5491	176
O (34,334)	22429–22540	14974–15003	7,426
		30126–30155	7,586

[a] The positions of the host and wasp motifs on each segment correspond to sequences submitted to GenBank (see Materials and Methods for accession numbers).

770 and 836 nt apart in segments C and G, respectively, while segment O contained two predicted WIMs that were separated from the predicted HIM by more than 7 kb (Table 1).

DISCUSSION

PDVs are specialized symbionts of wasps that function as replication-defective gene delivery vehicles in the insects (hosts) that the wasps parasitize. Our understanding of how PDVs alter the physiology of hosts for the benefit of wasp offspring has increased greatly in recent years (summarized in references 23, 32, and 41), yet little is known about the fate of PDV genomes in infected host cells. This reflects in large measure that parasitism results in the relatively rapid death of permissive hosts, which are usually consumed by the wasp's offspring 7 to 14 days after the adult oviposits (23). Thus, based on limited experimental data (28, 38), the assumption has generally been that PDV genomes persist in hosts as episomes, which is adequate for the transient expression of the viral gene products required for successful parasitism (41). However, the long-term detection of some PDV genomic DNAs in continuous cell lines (11, 14, 15, 17, 21, 40), together with data showing that genomic DNAs from GiBV and TrIV integrate into continuous cell lines of host origin (11, 15), raises the possibility that PDV DNAs may not persist as episomes in hosts. However, it is unclear from these cell culture studies whether all or only some PDV genomic segments are capable of integrating, how quickly integration occurs, and whether the expression of viral gene products responsible for specific functional alterations continues after integration. It is also unknown whether PDVs actually integrate into hosts after parasitism.

Our results indicate that all 15 genomic segments of the MdBV encapsidated genome exhibit long-term persistence in CiE1 cells. Our results also reveal that many MdBV genes continue to be expressed, including members of the *glc* gene family whose products block adhesion and cause persistently infected CiE1 cells to grow as a suspension culture. Lastly, our sequencing of multiple host-viral DNA junction clones demonstrates that segments C and J integrate into parasitized *P. includens*, while our PCR-based assays suggest that integration begins within 2 days of parasitism. Previous studies suggested

that the integration of proviral DNAs into wasps and the integration of episomal DNAs into host cell lines could be regulated through a shared integration site (15, 40). In characterizing integration into CiE1 cells, we determined that MdBV genomic segments contain a motif that has been identified in other BV isolates as the site of proviral DNA excision during replication in wasps (1, 10). Our results show that this WIM identifies the location on segments B, C, and J where integration into *M. demolitor* occurs but does not identify the site of integration into CiE1 cells or *P. includens*. Instead, our sequence data for segments C and J indicate that integration into hosts occurs at a second site that we call an HIM. The presence of an HIM in other MdBV segments further suggests that most, if not all, MdBV genomic DNAs also integrate into hosts, which is further supported by the long-term persistence of all MdBV genomic segments in CiE1 cells.

The single host-virus junction site for TrIV segment F cloned from spruce budworm-derived CF-124T cells provided no insights into how integration occurs (11). Somewhat similar to our findings, though, the integration of segment F is associated with a 33-nt deletion from the episomal DNA. The single junction site identified for integrated segment 25 from GiBV (formerly segment F [10]) in gypsy moth IPLB-LdEp cells showed that the viral boundary was defined by the sequence CATGGTAC (15). This sequence is palindromic, as are the sequences on each end of the HIMs identified in MdBV segments (Fig. 8). However, our own examination of GiBV segment 25 in the region associated with integration into IPLB-LdEp cells failed to identify a motif with homology to an MdBV HIM or that differed in sequence but formed a predicted stem-loop structure. We also did not identify a homologous HIM in other genomic DNAs from BVs of wasps in other genera that have been submitted to GenBank. However, genomic sequence data that we recently generated for BVs from other species of *Microplitis* do identify the presence of HIMs that are similar to those identified in MdBV (M. H. Beck, G. R. Burke, and M. R. Strand, unpublished data). Taken together, the similarity in WIMs among BVs from wasps in diverse subfamilies suggests an ancient origin and long-term conservation of proviral excision/integration motifs that may date back to the evolution of BVs from a nudivirus ancestor (6, 43). In contrast, our finding of MdBV-like HIMs on genomic segments of BVs from wasps in the genus *Microplitis* but not other genera suggests that either the common ancestor of *Microplitis* BVs acquired this domain or BVs in other taxa have partially or fully lost it.

Dissimilarities in the junction sequences that we cloned indicate that the integration of segments J and C may not be fully specific at the nucleotide level. On the other hand, our finding that three junction clones for segment J integrate into a similar location in the *P. includens* genome together with our qPCR and Southern blotting data also suggest that integration is not random and does exhibit a level of site specificity for a particular host target domain. The detection of multiple copies of segment J per CiE1 cell genome but only two novel hybridization signals on Southern blots suggests the possibility that the host target sequence that we identified exists in multiple copies and/or that segment J also integrates into another target site. In contrast, the detection of only one copy of segment C per host cell genome together with a single novel fragment on

Southern blots suggests that this viral DNA may integrate into a unique host target site. It is also possible that the higher copy number of segment J per host genome than that of segment C could reflect a greater molar abundance of segment J than that of segment C at the time of infection.

Our results suggest that MdBV segments integrate into the host genome through a similar mechanism. This mechanism could involve MdBV gene products expressed in *P. includens* (7). The absence of any predicted recombinase or endonuclease in the encapsidated genome, however, argues that integration also involves unknown host factors interacting with the HIM on different MdBV genomic segments and potentially specific host target sequences. Currently, the only known animal DNA virus to exhibit site-directed integration is adeno-associated virus (AAV), where nonhomologous recombination into different locations of the AAVS1 domain in human chromosome 19 involves interactions between virus-encoded proteins, palindrome-forming terminal inverted repeats in the viral genome, and host cell machinery (9, 18, 19, 24, 44). The integration of another group of parvoviruses (densoviruses) that infect insects may also involve unknown host cell factors interacting with viral sequences (8).

The inverted repeats of the HIMs on different MdBV genomic segments are clearly similar, but the loop domains differ (Fig. 8B). We speculate that these differences may play a role in where different MdBV segments integrate into the host genome. In contrast, our comparative data for host target sequences are insufficient to discern whether any common features exist. The junction site identified for GiBV segment 25 in IPLB-LdEp cells contained a small region with homology to a Pao-like retrotransposon and an open reading frame with homology to a polymerase, which Gundersen-Rindal and Lynn (15) speculated could play a role in integration. In contrast, we identified no significant homology in the host junction sequences from *P. includens* with any transposable element or genes in current databases. However, the host target site shown in Fig. 7A for segment J is strongly A+T rich, which is sometimes associated with nonhomologous recombination events in mammalian cells (18). Key future needs thus include determining what features of the HIM are required for integration, whether HIMs on different segments differ in their targeting preferences, and how this motif interacts with the recombination machinery of the host. *In situ* analysis will also be important in generating insights into the spatial distribution of different MdBV genomic DNA insertions into host chromosomes.

Since MdBV genomic segments integrate into *P. includens* before wasp offspring complete their development, we conclude that the integration of this PDV is a legitimate feature of parasitism and is not solely an event that occurs in continuous cell lines. However, at present, we can only speculate as to its functional significance. One previously proposed idea is that the integration of viral DNAs could alter or disrupt the expression of host genes that otherwise would adversely affect the survival of wasp offspring (15). A second idea is that integration ensures that viral DNAs persist and that associated viral gene products are produced in the latter stages of parasitism, which could also be important for the successful development of the wasp. While the progeny of most PDV-carrying wasps develop relatively rapidly, many species also diapause in their host, which extends the period required for progeny development in a host to a period of months. The integration of the PDV genome under such circumstances could thus be vital for the long-term persistence and expression of gene products required for successful parasitism. A third possibility is that the association between some PDVs and wasps may not be fully beneficial, with some PDV DNAs possessing selfish elements that facilitate horizontal movement in the absence of replication. Since PDV-carrying wasps sometimes parasitize nonpermissive or semipermissive hosts that can survive parasitism (23, 32), the ability of PDV genomic DNAs to rapidly integrate creates the potential for dissemination and persistence independent of the wasp.

REFERENCES

1. **Annaheim, M., and B. Lanzrein.** 2007. Genome organization of the *Chelonus inanitus* polydnavirus: excision sites, spacers, and abundance of proviral and excised segments. J. Gen. Virol. **8:**450–457.
2. **Beck, M., and M. R. Strand.** 2003. RNA interference silences *Microplitis demolitor* bracovirus genes and implicates glc1.8 in disruption of adhesion in infected host cells. Virology **314:**521–535.
3. **Beck, M. H., and M. R. Strand.** 2005. Glc1.8 from *Microplitis demolitor* bracovirus induces a loss of adhesion and phagocytosis in insect high five and S2 cells. J. Virol. **79:**1861–1870.
4. **Beck, M. H., and M. R. Strand.** 2007. A novel polydnavirus protein inhibits the insect prophenoloxidase activation pathway. Proc. Natl. Acad. Sci. U. S. A. **104:**19267–19272.
5. **Beck, M. H., R. B. Inman, and M. R. Strand.** 2007. *Microplitis demolitor* bracovirus genome segments vary in abundance and are individually packaged in virions. Virology **359:**179–189.
6. **Bezier, A., et al.** 2009. Polydnaviruses of braconid wasps derive from an ancestral nudivirus. Science **323:**926–930.
7. **Bitra, K., S. Zhang, and M. R. Strand.** 2011. Transcriptomic profiling of *Microplitis demolitor* bracovirus reveals host, tissue, and stage-specific patterns of activity. J. Gen. Virol. **92:**2060–2071.
8. **Bossin, H., et al.** 2003. *Junonia coenia* densovirus-based vectors for stable transgene expression in Sf9 cells: influence of the densovirus sequences on genomic integration. J. Virol. **77:**11060–11071.
9. **Daya, S., N. Cortez, and K. I. Berns.** 2009. Adeno-associated virus site-specific integration is mediated by proteins of the nonhomologous end-joining pathway. J. Virol. **83:**11655–11664.
10. **Desjardins, C. A., et al.** 2008. Comparative genomics of mutualistic viruses of *Glyptapanteles* parasitic wasps. Genome Biol. **9:**R183.
11. **Doucet, D., et al.** 2007. In vitro integration of an ichnovirus genome segment into the genomic DNA of lepidopteran cells. J. Gen. Virol. **88:**105–113.
12. **Dupuy, C., E. Huguet, and J.-M. Drezen.** 2006. Unfolding the evolutionary history of polydnaviruses. Virus Res. **117:**81–89.
13. **Fleming, J. G. W.** 1992. Polydnaviruses: mutualists and pathogens. Annu. Rev. Entomol. **37:**401–425.
14. **Gundersen-Rindal, D., and E. M. Dougherty.** 2000. Evidence for integration of *Glyptapanteles indiensis* polydnavirus DNA into the chromosome of *Lymantria dispar* in vitro. Virus Res. **66:**27–37.
15. **Gundersen-Rindal, D. E., and D. E. Lynn.** 2003. Polydnavirus integration in lepidopteran cells in vitro. J. Insect Physiol. **49:**453–462.
16. **Johnson, J. A., et al.** 2010. The UGA-CiE1 cell line from *Chrysodeixis includens* exhibits characteristics of granulocytes and is permissive to infection by two viruses. Insect Biochem. Mol. Biol. **40:**394–404.
17. **Kim, M. K., G. Sisson, and D. Stoltz.** 1996. Ichnovirus infection of an established gypsy moth cell line. J. Gen. Virol. **77:**2321–2328.
18. **Kotin, R. M., R. M. Linden, and K. I. Berns.** 1992. Characterization of a preferred site on human chromosome 19q for integration of adeno-associated virus DNA by non-homologous recombination. EMBO J. **11:**5071–5078.
19. **Linden, M. R., P. Ward, C. C. Giraud, E. Winocour, and K. I. Berns.** 1996. Site-specific integration by adeno-associated virus. Proc. Natl. Acad. Sci. U. S. A. **93:**11288–11294.
20. **Lu, Z., M. H. Beck, H. Jiang, Y. Wang, and M. R. Strand.** 2008. The viral protein Egf1.0 is a dual activity inhibitor of prophenoloxidase activating proteinases 1 and 3 from *Manduca sexta*. J. Biol. Chem. **283:**21325–21333.
21. **McKelvey, T. A., et al.** 1996. Transformation of gypsy moth cell lines by infection with *Glyptapanteles indiensis* polydnavirus. Biochem. Biophys. Res. Commun. **224:**764–770.

22. **Ochman, H., F. J. Ayala, and D. L. Hartl.** 1993. Use of polymerase chain reaction to amplify segments outside boundaries of known sequences. Methods Enzymol. **218:**309–321.

23. **Pennacchio, F., and M. R. Strand.** 2006. Evolution of developmental strategies in parasitic Hymenoptera. Annu. Rev. Entomol. **51:**233–258.

24. **Philpott, N. J., et al.** 2002. Efficient integration of recombinant adeno-associated virus DNA vectors requires a p5-rep sequence in cis. J. Virol. **76:**5411–5421.

25. **Pruijssers, A. J., and M. R. Strand.** 2007. PTP-H2 and PTP-H3 from *Microplitis demolitor* bracovirus localize to focal adhesions and are antiphagocytic in insect immune cells. J. Virol. **81:**1209–1219.

26. **Pruijssers, A. J., et al.** 2009. Infection by a symbiotic polydnavirus induces wasting and inhibits metamorphosis of the moth *Pseudoplusia includens*. J. Exp. Biol. **212:**2998–3006.

27. **Stoltz, D. B.** 1993. The PDV life cycle, p. 167–187. *In* S. N. Thompson, B. A. Federici, and N. E. Beckage (ed.), Parasites and pathogens of insects, vol. 1. Parasites. Academic Press, San Diego, CA.

28. **Stoltz, D. B., D. Guzo, and D. Cook.** 1986. Studies of polydnavirus transmission. Virology **155:**120–131.

29. **Strand, M. R.** 1990. Characterization of larval development in Pseudoplusia includens (Lepidoptera, Noctuidae). Ann. Entomol. Soc. Am. **83:**538–544.

30. **Strand, M. R.** 1994. *Microplitis demolitor* polydnavirus infects and expresses in specific morphotypes of *Pseudoplusia includens* haemocytes. J. Gen. Virol. **75:**3007–3020.

31. **Strand, M. R.** 2009. The interactions between polydnavirus-carrying parasitoids and their lepidopteran hosts, p. 321–336. *In* M. R. Goldsmith and F. Marec (ed.), Molecular biology and genetics of the Lepidoptera. CRC Press, Boca Raton, FL.

32. **Strand, M. R.** 2010. Polydnaviruses, p. 171–197. *In* S. Asgari and K. N. Johnson (ed.), Insect virology. Caister Academic Press, Norwich, United Kingdom.

33. **Strand, M. R., and T. Noda.** 1991. Alterations in the haemocytes of *Pseudoplusia includens* after parasitism by *Microplitis demolitor*. J. Insect Physiol. **37:**839–850.

34. **Strand, M. R., and L. L. Pech.** 1995. *Microplitis demolitor* polydnavirus induces apoptosis of a specific haemocyte morphotype in *Pseudoplusia includens*. J. Gen. Virol. **76:**283–291.

35. **Strand, M. R., D. I. McKenzie, V. Grassl, B. A. Dover, and J. M. Aiken.** 1992. Persistence and expression of *Microplitis demolitor* PDV in *Pseudoplusia includens*. J. Gen. Virol. **73:**1627–1635.

36. **Strand, M. R., R. A. Witherell, and D. Trudeau.** 1997. Two *Microplitis demolitor* PDV mRNAs expressed in hemocytes of *Pseudoplusia includens* contain a common cysteine-rich domain. J. Virol. **71:**2146–2156.

37. **Suderman, R. J., A. J. Pruijssers, and M. R. Strand.** 2008. Protein tyrosine phosphatase-H2 from a polydnavirus induces apoptosis of insect cells. J. Gen. Virol. **89:**1411–1420.

38. **Theilmann, D. A., and M. D. Summers.** 1986. Molecular analysis of *Campoletis sonorensis* virus DNA in the lepidopteran host *Heliothis virescens*. J. Gen. Virol. **67:**1961–1969.

39. **Trudeau, D., R. A. Witherell, and M. R. Strand.** 2000. Characterization of two novel Microplitis demolitor PDV mRNAs expressed in *Pseudoplusia includens* haemocytes. J. Gen. Virol. **81:**3049–3058.

40. **Volkoff, A.-N., et al.** 2001. Persistent expression of a newly characterized *Hyposoter didymator* polydnavirus gene in long-term infected lepidopteran cell lines. J. Gen. Virol. **82:**963–969.

41. **Webb, B. A., and M. R. Strand.** 2005. The biology and genomics of polydnaviruses, p. 323–360. *In* L. I. Gilbert, K. Iatrou, and S. S. Gill (ed.), Comprehensive molecular insect science, vol. 6. Elsevier, San Diego, CA.

42. **Webb, B. A., et al.** 2006. Polydnavirus genomes reflect their dual roles as mutualists and pathogens. Virology **347:**160–174.

43. **Whitfield, J. B.** 2002. Estimating the age of the polydnavirus/braconid wasp symbiosis. Proc. Natl. Acad. Sci. U. S. A. **99:**7508–7513.

44. **Yang, C. C., et al.** 1997. Cellular recombination pathways and viral terminal repeat hairpin structures are sufficient for adeno-associated virus integration in vitro and in vivo. J. Virol. **71:**9231–9247.

45. **Zuker, M.** 2003. Mfold Web server for nucleic acid folding and hybridization prediction. Nucleic Acids Res. **31:**3406–3415.